KeAi
CHINESE ROOTS
GLOBAL IMPACT

International Journal of Innovation Studies

THE INFLUENCE OF CU ON THE THERMAL AND MECHANICAL PROPERTIES AND MICROSTRUCTURE OF LEAD-FREE SN–5SB SOLDER ALLOY

Samia E. Attia Negm [a,b,] * and M. M. El-Hady[c]
[a] Department of Physics, Faculty of Science, Al-Azhar University, Nasr City 11884, Cairo, Egypt, Girls Branch
[b] Department of General Science – Physics Division, Ibn Sina National College for Medical Studies, P.O. Box No. 31906, Jeddah, 21418, Saudi Arabia
[c] Department of Physics, Faculty of Science, Al-Azhar University., Nasr City 11884, Cairo, Egypt.

Abstract

In this study, we investigated the effect of Cu addition on the thermal and mechanical behavior of a lead-free Sn-Sb5 solder alloy. The specific heat of the samples was studied with differential thermal analysis (DTA). The wettability of the prepared molten alloys was measured by evaluating the contact angle on various smooth surfaced substrates (glass, pure Al, pure Cu, and CuZn30 alloy). Contact angles were recorded photographically at 550K using (colophonic acid) as flux. Microhardness tests were performed as a function of temperature to calculate the effective activation energy of Sn-Sb and Sn-Sb-Cu solder alloys. The isothermal creep curves of the alloy samples were obtained by applying various constant stresses at a constant temperature of 480 K and then annealing the samples at a pre-threshold temperature (Tm/2). Microstructural studies of as-cast alloys after annealing treatment are reported, with the influence of cold working and creep testing on the structural changes and properties of Sn-Sb and Sn-Sb-Cu alloys.

Keywords: Annealing temperature, Lead-Free Solder Alloy, Creep, Micro-Hardness Wetting

Introduction

Traditional soldering techniques have become essential for connecting and packaging nearly all electronic devices and circuits. Sn-Sb alloys are considered to have great potential [1]. In Sn-Sb alloys with high Sb concentrations, intermetallic compounds such as SbSn precipitates are dispersed in the matrix. This results in a significant bond strengthening effect that reduces the creep rate at temperatures below 100 °C. Most of the studies conducted in this field mainly focused on the mechanical properties of bulk solder, such as [2,3]. B. Tensile properties [4] and creep properties [5, 6]. The wetting reaction between Sn5Sb solder and Cu substrate plays an important role in the reliability evaluation of package structures. Chan et al. [1] investigated the wetting behavior of different SnSb alloys on Cu foil. Their results showed that the wetting angle decreased as the reflow time increased and varying the Sb content from 5% to 15% had no obvious effect on the wetting angle. Mechanical, electrical, and thermal properties. Sn-5Sb solder is one of the potential alternative materials to replace Pb-containing alloys [1].

One of the most important issues in the design and reliability evaluation of solder connections is the mechanical properties of the solder alloy. Therefore, the selection of solder is very important when it comes to the quality of the connection and the reliability of the assembly. In recent decades, lead-containing solders have been widely used for soldering in electronic applications due to their acceptable mechanical properties such as good corrosion resistance, high creep properties, low eutectic temperature, good wettability, and low cost. [7-9] Compared with traditional Sn-Pb solder, Sn-Cu alloy has attracted attention due to its excellent solderability, low melting point, reasonable cost advantages, good flowability, and narrow crystallization temperature range [10,11].

In this study, we investigated the effects of Cu on the microstructure, melting temperature, heat of fusion, and creep properties of lead-free Sn-5Sb solder alloys. The wettability of the prepared molten alloys was measured by evaluating the contact angle on various smooth surfaced substrates (glass, pure Al, pure Cu, and CuZn30 alloy). Contact angles were recorded photographically at 550K using (colophonic acid) as flux. A reference steel ball was used to check exposure angle, photo development, and printing accuracy. The creep characteristics of Sn-5wt%Sb solder alloy at two different annealing temperatures were experimentally investigated and discussed.

2. Experimental

2.1Sample Preparation

The samples were made from high-purity elements (99.99% tin, antimony, and copper by weight percent). The weight of the sample was determined using a sensitive microbalance with an accuracy of 10−4 grams. The weighed samples were placed in clean Pyrex tubes under a natural flux (rosin) of chemical components (abietic acid) to prevent sample oxidation in air and improve mixing and melting. Sample synthesis was carried out over 20 min in a benzene fire with tube shaking to ensure homogenization of the melt. After solidification, the tube was split to obtain a bulky alloy. Excess flux was removed by soaking the billet in pure carbon tetrachloride (CCl4) for sufficient time. The density of the prepared samples was determined by displacement method using carbon tetrachloride (CCl4, □ = 1.595 g/cm3) as the immersion liquid. Sample density was calculated using the following formula:

(1)

where, W is the weight of the sample and □ is the density.

3. Results

3.1 Bulk Density Measurements

The value of the experimental (□exp) bulk density for the (lead-free) low melting point binary alloys used in the present work were determined and given in Table (1). While the calculated density and the porosity percentage was calculated as follows:

□cal = [weight percent x density element (1)]+[weight percent x density element (2)]

$$Porosity\% = 1 - \frac{\rho_{exp}}{\rho_{cal\cdot}} \text{ x } 100 \qquad (2)$$

As shown from Table (1) the results proved that the present preparation procedure is adequate concerning these alloys.

Table 1

Densities, porosity, Melting Point, enthalpy, and Specific heat of the Sn-Sb solder alloys

Alloy	Density calculated	Density Experimental	Porosity %	M.. P (K)	ΔH (cal./gm)	Specific heat	
						Temperature(K)	Cp (J/kg. K)
$Sn_{95}Sb_5$	7.1	7.03	0.01	511	5.91	450	216.7
$Sn_{94.3}Sb_5Cu_{0.7}$	7.3	7.11	0.03	490	5.42	430	223

3.2 Thermal Analysis

3.2.1 Differential Thermal Analysis (DTA) Measurements

Melting temperature is an important solder property because it determines the maximum operating temperature of the system and the minimum processing temperature that its components must withstand. The DTA results are used to obtain information about the melting or solidification behavior of the alloy. For example, liquidus and solidus temperatures are extracted from data collected during liquidus or solidus operation. Two characteristic phenomena are observed in the DTA thermogram. The first one corresponds to the melting temperature Tm and corresponds to the intersection of two straight line segments adjacent to the transition shoulder of the DTA in the endothermic direction. The second is related to the melting transition region (endothermic region). The differential thermal analysis thermograms of eutectic alloys (Sn-Sb5 and Sn-Sb5-Cu0.7) are shown in the figure. (1a, b) or Figures show the melting points of Sn-Sb and Sn-Sb-Cu alloys from Table (1).

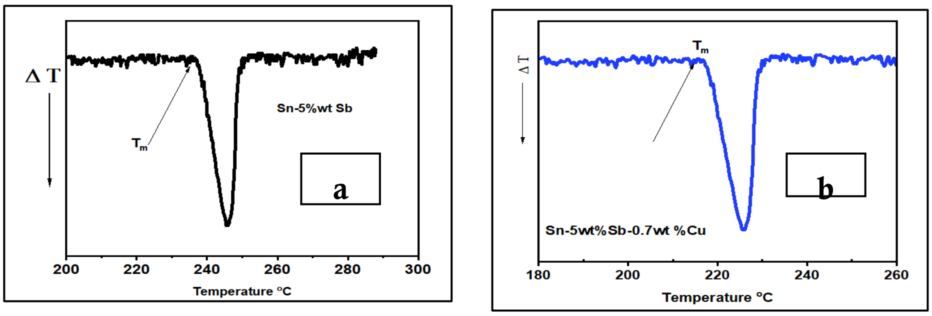

Fig. (1): The DTA thermograms of (a) Sn-Sb5 (b) Sn-Sb5-Cu0.7 solder alloys.

3.2.2 Calculation of the Latent Heat of Fusion

Thermal stability was investigated by calculating the enthalpy released during the transformation process, i.e. Latent heat of fusion. Experimental evaluation of the enthalpy (□H) during the melting process was determined from the calibration curve of DTA by measuring the area under the DTA peak and using indium and bismuth as standards (□Href). Applying the formula:

$$\Delta H = \Delta H_{ref}\, A/M \qquad (3)$$

where A is the area under the DTA peak and M is the mass of the sample. The calculation results of enthalpy □H of Sn-Sb5 and Sn-Sb5-Cu0.7 alloy are shown in Table (1).

3.2.3 Specific Heat Measurements

To measure the specific heat of the samples, a Newtonian cooling experiment with Al2O3 as the reference material was used.

$$C'_p = \frac{\left[m\, C''_p \frac{dT}{dt} \right]_{Al_2O_3}}{m \left[\frac{dT}{dt} \right]_s} \qquad (4)$$

where is the specific heat of the sample, is the specific heat of Al2O3, m is the mass in gm and dT/dt is the temperature gradient.

A Pyrex tube (4 mm diameter) was used as a measuring cell. The tube was inserted into a vertical oven. An AC control transformer was used to control the heating current. Temperatures were recorded with an accuracy of ±0.5°C using an automatic computer circuit. The temperature of the powder sample in the oven was measured using a calibrated thermocouple (nickel-chromium type K) with a diameter of 0.07 mm placed on the measuring sample of approximately 0.17 gm to ensure a high degree of reaction. After the sample reached a high temperature of 350 °C, it was removed from the oven and cooled independently to room temperature in a large cylindrical cavity. The same procedure was performed on the same weight of Al2O3 powder and used as a reference sample. Several properties determine the overall effect of applying heat to a metal or alloy. For example, the specific heat Cp controls the temperature rise □T that results from adding a given amount of heat Q to one kilogram of metal [12.13]:

$$Q = Cp\Delta T \qquad (5)$$

The specific heat of the alloy studied is That's right. It was evaluated according to Newton's cooling hypothesis [15]. The specific heat versus temperature and temperature-time cooling curve of Sn-5wt.%Sb are shown in the figure. (2 a, b), the liquidus point is 511 □1 K.

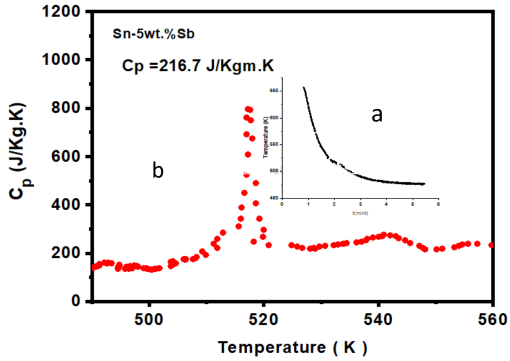

Fig. (2): a) The specific heat curves versus temperature together with b) The temperature-time cooling curves for Sn-Sb5.

Specific heat results at selected temperatures for Sn-Sb5 and Sn-Sb5-Cu0.7 alloys from Dulong and Petit are shown in Table (1). For an alloy to be valuable as a solder in the electronics industry, it must have certain properties, such as melting range. The liquidus temperature must be low enough so that the components and circuit board are not damaged during soldering (above which they will melt completely). (5) The specific heat of the investigated alloys was evaluated according to the Newtonian cooling hypothesis [15]. The specific heat versus temperature and temperature-time cooling curve of Sn-5wt.%Sb are shown in the figure. (2 a, b), the liquidus point is 511 □1 K .

3.2.4 Wettability Measurements

One of the most important applications of the studied alloys is that they can be used as filler metals in low-temperature applications. Wettability conditions should be investigated. Wettability is defined as the tendency of liquid metal to spread over a solid surface, and is a precursor to "solderability," which refers to the solder's ability to form an actual connection on a circuit board. This is quantitatively evaluated based on the contact angle that occurs at the solder-substrate-air or flux triple points [14,15]. To optimize the operational performance of the joint, it is also important to correlate the microstructure of the alloy with its mechanical properties (tensile strength, fatigue resistance, creep resistance) [16]. Wettability is quantitatively evaluated by the contact angle formed at the solder-substrate-flux triple point. Solder wettability was measured based on the contact angle, base diameter, and height of the molten solder ball alloy. In this case, a flux (colophonic acid) is used to coat the solution during the production of molten alloy, which is like real conditions in industrial applications. A steel ball was used as a reference to check the accuracy of the angle of exposure, development, and printing of the photographs.

Figures (3) shows the wetting behavior of binary molten alloys prepared on different substrates (Cu, CuZn30, Al, glass) after 60 s at a temperature of 550 K. Over time, glass substrates were chosen to resemble dielectrics. The contact angles measured from the numerical values of the used Sn-Sb5 and Sn-Sb5-Cu0.7 alloys have the values listed in Table (2). The results show that the contact angle of the alloy on Cu and CuZn30 substrates is in the range of 37–42°, suggesting that this alloy melt can be used for soldering or plating brass objects. Even Sn-5 wt% Sb-0.7 wt% Cu is sufficient to be considered in the development of prototype solder connections in microelectronic packaging [17].

Table 2

Contact angles of the alloys on different substrates after 60 s elapsed time, Room temperature Vickers hardness numbers and activation energies of the Sn-Sb solder alloys.

Alloy	Contact angles at temperature 550 K				Vickers hardness numbers	
	Glass substrate	Al substrate	Cu substrate	CuZn30 substrate	HV. at R.T. (N/mm2)	Activation energy (kJ/mole)
Sn95Sb5	116	112	39	37	135.3 ±6	5.03
Sn94.3Sb5Cu0.7	119	114	40	42	115.4 ±11	5.96

3.3 Mechanical Properties

The characteristics of the mechanical properties of a material is strength, elasticity, ductility, creep, and hardness. Each of these is associated with the ability of the material to resist mechanical forces.

3.3.1 Microhardness Measurements

Microhardness tests are performed to measure the hardness of individual grains, phases, and structural components of alloys. In this case, the volume deformed by the indentation must be smaller than the volume of the particle being tested. Therefore, some force is applied to the indenter [18]. In this study, microhardness measurements of the samples were performed using a Vickers Shimadzu microhardness meter. This involves forcing a square diamond pyramid (with an angle of 136° between opposing surfaces) into the ground or polished surface being tested. The depth or size of the resulting indentation is measured, and this is related to the hardness value. The softer the material, the larger and deeper the depression, and the lower the value of the hardness index. The Vickers hardness number HV was determined using the following formula [19]:

$$H_V = \frac{2P\sin\frac{\alpha}{2}}{d^2} = 1.8544\,\frac{P}{d^2}\ \text{(kg/mm}^2\text{)} \qquad (6)$$

where P is the applied load and α is the angle between opposite faces of the diamond inventor (α = 136o), and d is the average length of the two diagonals of the indentation, in mm, measured, after removing the load, by means of a micrometer microscope.

In the present study, the applied load was 50 g for 5 s, and seven measurements of different indentations were performed at room temperature, the average value was obtained, and the standard deviation was calculated. Before indentation testing, it is essential to carefully prepare the sample surface (a flat parallel surface) and grind and polish it to obtain a smooth surface. The results obtained for the low-load microhardness values (according to Equation 6) of the pure metals Sn, Sb, Cu and their various alloys at room temperature are shown in Table (2). Some materials (e.g. metal) is constant above a critical indentation size, but below this size the microhardness increases steadily as the load decreases. Buckle [20.21] suggests that the presence of covalent bonding regions in such materials is responsible for the increase in hardness with decreasing stress. Several explanations have been proposed for the higher microhardness values at higher loads. McClintock and Argon [22] claim that at low loads, the size of the indentation approaches the length of the sliding strip at equivalent strain and the hardness value increases. Furthermore, the strain gradient around the imprint may require a higher dislocation density than that typically occurs in cold-worked metals at comparable strain levels. Meyers and Chawla [23] point out that the work hardening introduced into the surface by polishing can become important at higher loads. Dieter [24] claims that the impression at higher loads is significantly influenced by low elastic recovery, which is usually negligible at higher loads. Braunovic [25] proposed that the mechanism of load dependence of indentation hardness is related to the movement of dislocations caused by the indenter. The formation of dislocations on the contact surfaces can be expressed as the result of a punching mechanism. This movement can be hindered by the trapping and blocking of dislocations by lattice defects such as grain boundaries, vacancies, solutes, precipitates, and similar defects in crystalline solids.

3.3.2 Hot Hardness

Hardness measurement during heating (high temperature hardness measurement) is important for testing various qualities of heat-stable and heat-resistant structural materials. Factors that can affect these measurements include: The localized cooling caused by the cold indenter can significantly change the measured hardness, thus affecting the accuracy of the measurements. Significant errors can also be caused by oxidation on the sample surface. Oxidation occurs when heated in an oven without a protective atmosphere and becomes more pronounced as the temperature increases [18]. When a metal becomes hot, virtually all the supplied energy is absorbed by the ions rather than the valence electrons, increasing the vibrational amplitude of the ions. The crystal expands to a new equilibrium ionic distance, the interatomic distance over which bonding forces act increases, and the metal becomes more open and softer [26]. As the temperature increases, the distance increases and eventually the bonding forces can no longer ensure cohesion and the metal melts. A high melting point means high cohesion and hardness. The relationship between the Vicker hardness numbers according to Eqn. (7) as a function of temperature for the Sn-Sb5 and Sn-Sb5-Cu0.7 alloys is shown in the figure. (4a and b). From the figure, adding a small amount of Cu to Sn-Sb increases the Vicker hardness and improves the mechanical properties compared to pure Sn and Sb elements. The microhardness decreases exponentially with increasing alloy temperature. This means that heating can soften it, reducing its mechanical properties and reducing its wear resistance.

An Arrhenius equation describe the obtained results quite well and is given as:

$$H_V(T) = H_{V_o} \exp(Q/kT) \qquad (7)$$

where HV(T) is the hardness under thermal condition, HVo is the hardness of the initial state, k is the Boltzman constant, and Q may be described as the activation energy associated with thermal softening of the material.

As a measure of microhardness, we plotted the logarithm of the hardness of the data obtained from the figure. (4a and b) Values versus the reciprocal of the absolute temperature would be a straight line for alloys according to Eqn. (7) as shown in Figure (5a and b). The softening activation energy Q of pure metals and their alloys was calculated from the slope of these straight lines and summarized as shown in the Table. (2).

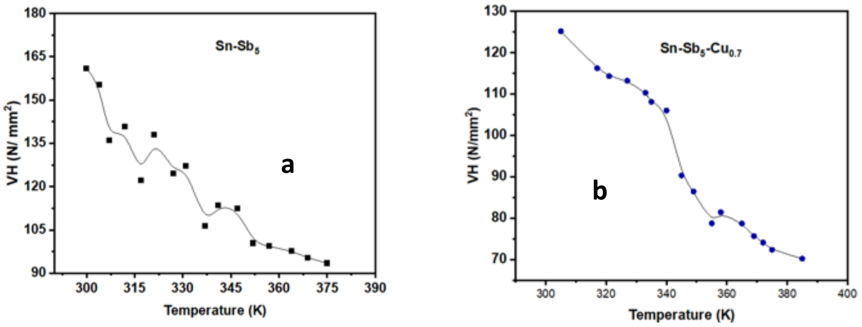

Fig. (4): The relation between the Vicker hardness number as a function of temperature for Sn-Sb5 and (b) Sn-Sb5-Cu0.7 alloys

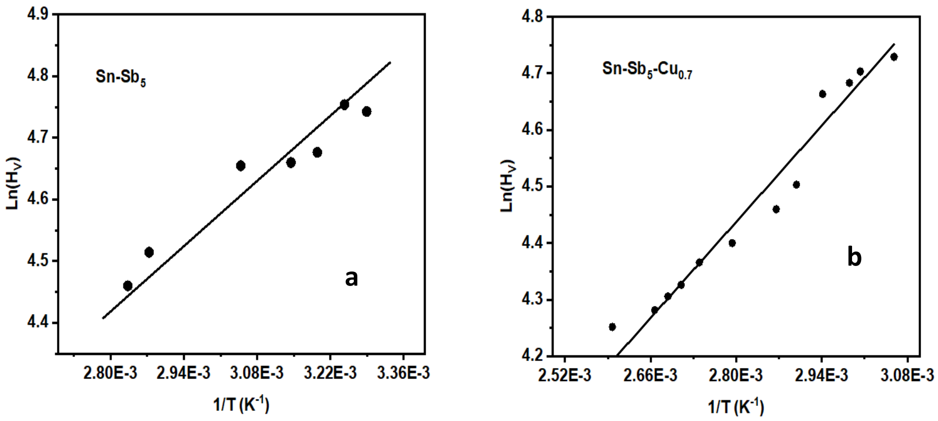

Fig. (5): Variation of the Vickers hardness number as a function of (1/T) according to Arrhenius equation for
a) Sn-Sb5 and b) Sn- Sb5-Cu0.7 alloy.

3.3.3 Creep Results

Modern technological advances require materials to be used at higher temperatures. One of the most important factors when considering such applications, and perhaps one of the most important, is creep behavior. The traditional method to study this creep is to subject a tensile sample to a constant load at a constant high temperature T and record its elongation □ versus time t. In some cases, the load may be automatically adjusted during stretching so that the average stress σ remains constant across the reduced section. This adjustment has limited value because it can hardly compensate for the variations in stress and strain at different points within the deforming grain [14]. Sn-Sb5 and Sn-Sb5-Cu0.7 creep samples were fabricated in the form of ribbons using melt-spinning technique (to obtain ribbons with good shape, the surface speed of the aluminum wheel was approximately 18.65 m/s). The rapid melt-spun ribbon samples were first annealed at 440 ± 2 K for 1 hour. The creep curves of rapid melt-spun ribbon Sn-Sb and Sn-Sb-Cu alloys were obtained at constant test temperature and different stress are shown in the figure. (6a,b). The creep process under constant load is highly temperature dependent. The observed creep behavior has three characteristic stages. There is an initial (unsteady) creep region where the creep rate changes rapidly, followed by a region where the creep rate remains constant (steady-state creep), and finally a third region where the creep rate increases rapidly, and which is followed by failure. The creep behavior observed at each stress level was of normal type, i.e., a rapid increase in strain (instantaneous strain □o), followed by a decrease in strain rate over time (primary creep), followed by a long period of creep at a constant strain rate (secondary creep). and finally, this (tertiary creep). This nomenclature assumes that the creep curve has four stages, with the instantaneous strain often referred to as the first stage of creep [27]. Such behavior is typical of both pure metals and many M-class creep alloys. Previous analyzes have shown that stress levels are high enough to allow dislocations from the resistance of solute atoms, which explains why the solid solution strengthened alloy exhibited class M creep behavior [28]. Creep properties are primarily determined by temperature, composition, and microstructure. The microstructures of Sn-Sb and Sn-Sb-Cu alloys after creep tests are shown in Figures (6a and b). The effect of deformation after creep testing on the microstructure of alloys with large grain sizes is indicated by the elongation of the grains compared to before creep testing. By performing creep tests up to the melting point, it was found that melting of the alloy does not substantially affect the creep behavior of the alloy. The irregular creep behavior of this alloy was attributed to its microstructure. An indication for the three stages (transient, steady-state and tertiary), the plot of the strain rate vs. are shown in fig. (7) for Sn-Sb as example. The variation in strain rates (creep rates) is the result of changes in the internal structure of the material with creep strain and time.

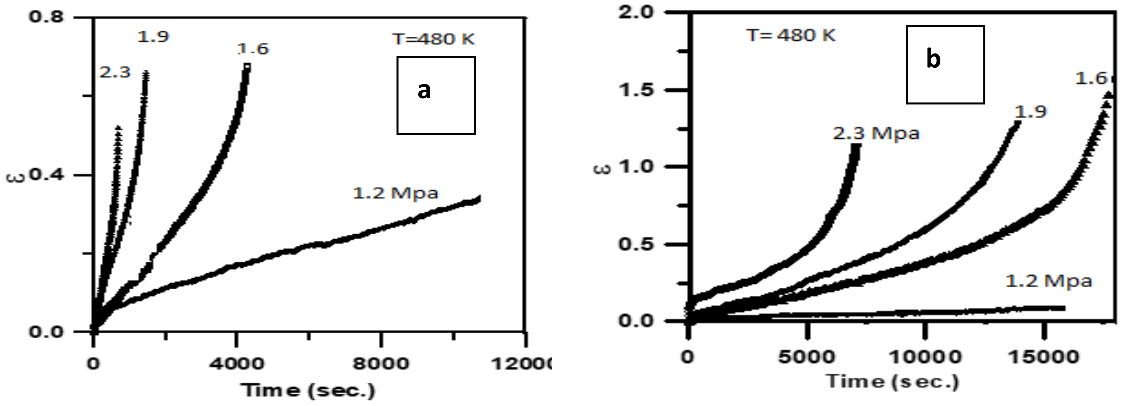

Fig. (6): Isothermal creep curves under different stress and annealing temperature (440□2K) for (1 hr) for
(a)Sn-Sb and b) Sn-Sb-Cu solder alloys in ribbon form.

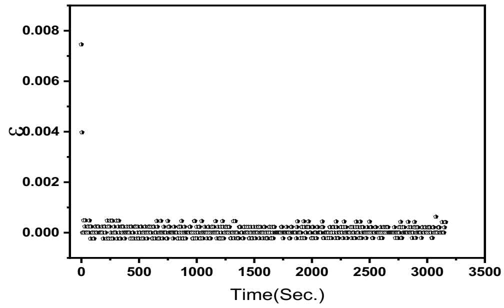

Fig. (7): The differential creep curves for
Sn-Sb5 solder.

3.3.4 Microstructure of the as Cast Alloys

Microstructural studies of solder alloys clearly show the differences between the two alloys tested, Sn-Sb5 and Sn-Sb5-Cu0.7, in terms of composition and processing. When an etching reagent is applied to the polished surface of a metallographic sample, structural details become partially visible through a process that selectively degrades the structure from the surface downward. This type of representation of metal structures is possible because the different components of a multiphase alloy, or the cut planes of differently oriented grains of a pure metal or single-phase alloy, are typically treated with disparate etching reagents. This is because it has a high dissolution rate. The active property of some reagents is to selectively discolor or stain certain phases of the structure, in addition to revealing structural details through preferential dissolution [29]. In general, microstructural changes and the formation of new IMCs within the matrix alloy can increase the strength and decrease the ductility [30]. Microstructure of the interface between a copper substrate and lead-free SnSbCu solder after wetting at 623 K and 1800 s, and of a copper solder-copper joint prepared under the same conditions, melting and solidification of the solder. We studied this phenomenon together [31].

The microstructure of the as-cast Sn-Sb5 alloy after an annealing temperature of 440 □2 K is shown under magnification (500x) in Figure (8a). The precipitated phase usually solidifies in the form of large particles, which is related to the peculiarity of the growth of the precipitated phase when the solidification of the alloy proceeds within the temperature range between the liquidus and solidus.

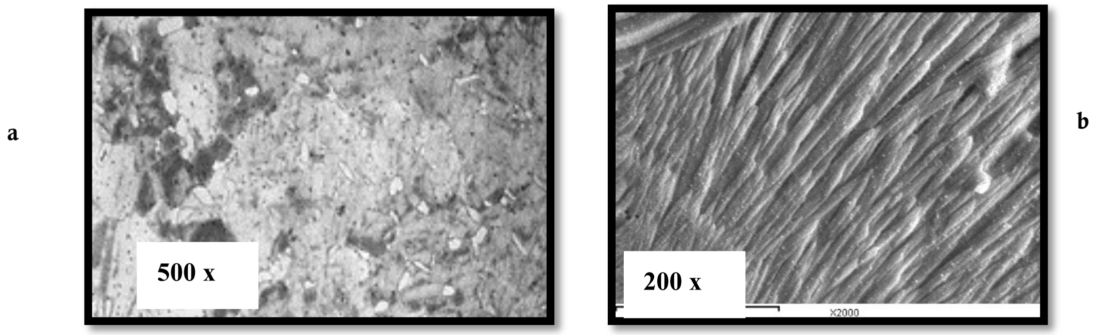

Fig. (8): Microstructure of (a) Sn-Sb5 and (b) Sn-Sb5-Cu0.7 as-cast after annealing at 440 □ 2 K for 1 hr.

The microstructure of the original as-cast state of the Sn-Sb5-Cu0.7 alloy after annealing at a temperature of 440 □2 K for one hour is shown in Fig. (8b). Micrographs show that this alloy consists of nearly pure Sn with rod-like intermetallic Ag3Sn or dendritic eutectic mixture in a pure Sn matrix, and intermetallic Ag3Sn precipitates in a pure Sn matrix. [32]. This annealing temperature affects the shape of the dendritic eutectic mixture. The region between the Sn dendrites consists of a layered two-phase eutectic structure of the Sn parent phase and the intermetallic compound Cu3SnSb phase. The structure of the bulk sample after annealing temperature (440 □2 K) is shown in the figure. (8). The figure (8) shows the structure before the creep test (after cold work) at an annealing temperature of 440□2K for one hour. Cold deformation fragmented the dendrites and aligned them along lines. Figure (8a) also shows the metallographic micrograph of the Sn-Sb5 alloy creeping under stress (2.3 MPa) at a test temperature of 480 K (500x magnification). The structure after creep contains □-Sn dendrites aligned along the tensile axis, but the orientation of the structure is lower than before tensile deformation. When the ingot size is very large, the effect of high deformation after the creep test on the microstructure of the alloy is indicated by the elongation of the grains compared to before the creep test in Figure (8a). The metallographic micrograph of the eutectic Sn-Sb5-Cu0.7 alloy before creep test (cold deformation 94.5%) at an annealing temperature of 440□2K is shown in Figure (8b) (200x magnification). The crystal lattice is distorted and the initial blocks of equiaxed particles are broken to produce thin plates.

Figure (9a) shows the microstructure of Sn-Sb5 alloy after cold working. The structure of the alloy after a low annealing temperature 440□2K after creep at a stress of 2.3 MPa, significant coarsening of the grains was observed due to deformation [23]. The density of Sn-Sb intermetallic particles in the matrix was also reduced due to grain boundary segregation and/or dissolution of Sn-Sb intermetallic compounds. However, when deformation occurs due to the creep test, the shape of the crystal grains changes as shown in Figure (9b). The microstructure of the Sn-Sb5-Cu0.7 eutectic sample crept under stress (2.3 MPa) and test temperature 480 K is shown in Figure (9b), magnification 200x. The observed decrease in grain size may be due to the formation of dislocation clusters at grain and phase boundaries. Since the creep temperature is in the two-phase region, the system still consists of two phases: □ phase (Sn-rich phase). □ phase (Sb-rich phase) and (Cu-rich phase). This can disrupt the boundary continuity and cause particle segmentation [33], and a decrease in particle diameter is observed as previously shown [34]. The pure Sn phase is much softer than the eutectic structure, and the uneven distribution of such phases can contribute to creep failure. The presence of Sn dendrites also indicates the non-equilibrium cooling rate used in sample preparation [35]. Under the same conditions, alloys that have formed a fine-grained structure through (primary) recrystallization will experience significant grain growth when heated to higher temperatures. This mechanism involved rapid movement of the boundaries of some primary recrystallized grains, resulting in the consumption of a large portion of the primary grains and the production of very large secondary grains. Other names for these phenomena are discontinuous grain growth and anomalous grain growth [7].

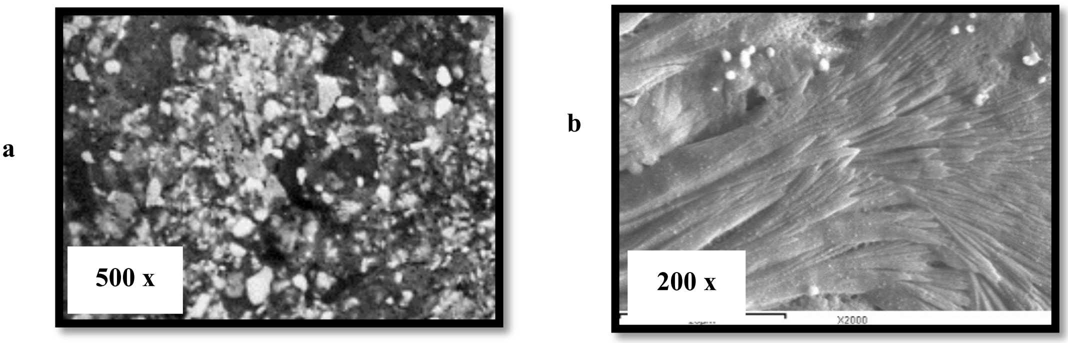

Fig. (9): Microstructure after creep for a)Sn-Sb b) Sn-Sb-Cu

Conclusion

In this study, two low melting point alloys, consisting of alloys Sn-Sb5 and Sn-Sb5-Cu0.7, were melted with weighed sample components in a Pyrex tube under a flux (colophonic acid) to prevent melt oxidation in air. Home-made computer-based circuits for differential thermal analysis (DTA), latent heat of fusion, specific heat, and creep were used for measurements. The results can be summarized as follows:

The melting points of solder alloys (Sn-Sb) and (Sn-Sb-Cu) were determined using both differential thermal analysis (DTA) measurements and specific heat.

From the DTA measurements, the heat of fusion (□H) during the melting process was calculated and the values for the alloy were 5.91 and 5.42 cal/g.

The specific heat of two binary tin alloys according to the Dulong-Petit criterion increases with temperature.

Wetting contact angles of three alloys were measured as droplets on various smooth substrates. The results show that the contact angles on Cu and CuZn30 substrates range from 37° to 42°, while those on Al and glass substrates range from 112° to 119°. This means that the alloy melt can be used for soldering and plating brass products.

Microhardness measurements at room temperature were calculated to be 115.4 ±11 N/mm2 and 135.3 ±6 N/mm2 for Sn-Sb5 and Sn-Sb5-Cu0.7 alloys, respectively. Additionally, the microhardness measurements can be fitted to an Arrhenius function (ln HV vs. 1/T) with temperature, and the thermally activated softening.

energies are 5.96 and 5.03 kJ/mol for Sn-Sb5 and Sn-Sb5-Cu0.7

Isothermal creep curves were measured for Sn-Sb5 and Sn-Sb5-Cu0.7 at a constant temperature of 480 K and different stresses ranging from 1.2 to 3.2 MPa. The creep behavior observed at each stress level was normal at four different stages.

The microstructures of the original as-cast Sn-Sb5 and Sn-Sb5-Cu0.7 alloys appear as a lameller two-phase and globular structures, respectively, after an annealing temperature of 440 K. After the creep test of Sn-Sb5 alloy, the block size becomes much larger and the grains are more elongated than before the creep test.

In the micrograph study of Sn-Sb5-Cu0.7 alloy after creep test, the boundary continuity can be disturbed, grain cleavage occurs, and a decrease in grain size can be observed. The microstructure of as-cast Sn-Sb5 alloys shows that the precipitated phase usually solidifies in the form of large grain of the alloy and progresses within the temperature range between liquidus and solidus. Comparing the microphotographs after the two annealing temperatures showed that the grains of the alloy heated to the higher temperature were coarser. After cold working at high annealing temperature (before creep test), the grain shape and its size changed, and discontinuous grain growth and abnormal grain growth were clearly noticeable at 95% Tm. After the creep test, the density of Sn-Sb intermetallic particles in the matrix decreased due to grain boundary segregation or dissolution of SnSb intermetallic compounds at low annealing temperatures, and the shape of the grains changed after high-temperature annealing.

Funding

This research received no external funding.

Declaration of competing interest

The author declares that she hasn’t known competing financial interests or personal relationships that could have appeared to influence the work reported in this paper.

References

[1] A. M. El-Tahe , H. M. Abd Elmoniem , and S Mosaad,J Mater Sci: Mater Electron (2023) 34:59

[2] S. Chen, P. Chen, C. Wang, J. Electron. Mater. 35 (2006) 1982.

[3] R. McCabe, M. Fine, Metall. Mater. Trans. 33A (2002) 1531.

[4] R. Mahmudi, A. Geranmayeh, A. Rezaee-Bazzaz, Mater. Sci. Eng. A 448 (2007) 287.

[5] M. Kerr, N. Chawla, JOM 65 (2004) 50.

[6] D. Joo, J. Yu, S. Shin, J. Electron. Mater. 32 (2003) 541.

[7] H. Huang, B. Chen, X. Hu, X. Jiang, Q. Li, Y. Che, S. Zu, D. Liu, J. Mater. Sci. 33, 15586–15603 (2022)

[8] L. Xu, X.H. Jing, L. Wang, J. Wei, Y. Han, Mater. Sci. Eng. A 667, 87–96 (2016)

[9] A.A. El-Daly, A.M. El-Taher, S. Gouda, Mater. Des. 65, 796–805 (2015)

[10] A. Ghosh, K. Mandal, Phys. Proc. 54, 10–15 (2014)

[11] W.R. Oso´ rio, J.E. Spinelli, C.R.M. Afonso, L.C. Peixoto, A. Garcia, Electro. Acta 56, 8891– 8899 (2011)

[12] G. Albert Guy and J. John Hren, “Elements of Physical Metallurgy”, Addision-Wesley Publishing Company, 1974.

[13] J. Kumaraswamy, Vijaya Kumar, G. Purushotham, A review on mechanical and wear properties of ASTM a 494 M grade nickel-based alloy metal matrix composites, Mater. Today Proc. 37 (Part 2) (2010).

[14] W. A. Wood, “The Study of Metal Structure and Their Mechanical Properties”, Pergamon press New York, 1971.

[15] R. K. Mahidhara, S. M. L. Sastry,K. L. Jerina,I. Turlik and K. L. Murty, J. Mater. Sci. Lett., 13, 1387 (1994).

[16] P.T. Viaco and J.A. Rejent, J. Electron. Mater., 28, 1138 (1999).

[17] R. K. Mahidhara, S. M. Sastry, Iwona Turlik and K. L. Murty, Scr. Metall. Mater., 31, 1145 (1994).

[18] Yu. A. Geller and A. G. Rakhshtadt, “Science of Materials”, Mir Publishers Moscow, 1977.

[19] Yuri Lakhtin, “Engineering Physical Metallurgy and Heat-Treatment”, Mir Publishers Moscow, 1974.

[20] Manoj Gupta, Introduction to metal matrix composite materials, in: Dermot Brabazon (Ed.), Encyclopedia of Materials: Composites, Elsevier., Amstredam, 2021.

[21] H. Buckle, Met. Rev. 4, 49 (1959); reference [84].

[22] I. S. Virk, M. B. Winnicka and R. A. Varin, Scr. Metall. Mater., 24, 2181 (1990).

[23] M. A. Meyers and K. M. Chawla, in Mechanical Metallurgy – principles and applications, Prentice-Hall, Inc., Englewood Cliffs, New Jersey (1984); reference [87].

[24] G. E. Dieter, in Mechanical Metallurgy, p.335, McGraw-Hill Book Co., New York (1986).

[25] M. El-Bahay, M. El-Mossalamy, M. Mahdy, A. Bahgat, Phys. Stat. Sol. A 198 (2003)

[26] G. Zeng, S.D. McDonald, Q. Gu, Y. Terada, K. Uesugi, H. Yasuda, K. Nogita, Acta Mater. 83, 357–371 (2015)

[27] E. George Dieter, “Mechanical Metallurgy”, McGraw-Hill Book company, New York, 1988.

[28] M. J. Davidson, M. Biberger, and A. K. Mukherjee, Scr. Metall. Mater. 27, 1829 (1992).

[29] C.T. Wang, H. Yong, T.G. Langdon, Acta Mater. 185, 245–256 (2020)

[30] M. Ghosh, M.K. Gunjan, S.K. Das, A. Kar, R.N. Ghosh, A.K. Ray, Mater. Sci. Technol. 26, 610–614 (2010)

[31] P. Sebo , P. Sve , D. Janickovi, E. Illeková, Yu. Plevachuk, Materials Science and Engineering A ˇ 528 (2011) 5955–5960

[32] D. R. Flanders, E. G. Jacobs and R. F. Pinizzotto, J. Electron. Mater., 26, 883 (1997).

[33] Y. Tang, S.M. Luo, W.F. Huang, Y.C. Pan, G.Y. Li, J. Alloys Compd. 719, 365–375 (2017)

[34] A.A. El-Daly, Y. Swilem, A.E. Hammad, Journal of Alloys and Compounds 471 (2009) 98–104

[35] M. McCormack and S. Jin, J. Electron. Mater. 24, 635 (1994).